Co-stimulation of CD28/CD40 signaling molecule potentiates CAR-T cell efficacy and stemness

Wannakorn Khopanlert,[1,2,3] Pongsakorn Choochuen,[2,4] Kajornkiat Maneechai,[1,2,3] Nawaphat Jangphattananont,[1] Socheatraksmey Ung,[1,2] Shingo Okuno,[5] Peter Steinberger,[6] Judith Leitner,[6] Surasak Sangkhathat,[2,4] Pongtep Viboonjuntra,[1] Seitaro Terakura,[5] and Jakrawadee Julamanee[1,3]

[1]Stem Cell Laboratory, Hematology Unit, Division of Internal Medicine, Faculty of Medicine, Prince of Songkla University, Hat Yai, Songkhla 90110, Thailand; [2]Department of Biomedical Sciences and Biomedical Engineering, Faculty of Medicine, Prince of Songkla University, Hat Yai, Songkhla 90110, Thailand; [3]Thailand Hub of Talents in Cancer Immunotherapy (TTCI), Bangkok, Thailand; [4]Translational Medicine Research Center, Faculty of Medicine, Prince of Songkla University, Hat Yai, Songkhla 90110, Thailand; [5]Department of Hematology and Oncology, Nagoya University Graduate School of Medicine, Nagoya 466-8560, Japan; [6]Division for Immune Receptors and T Cell Activation, Institute of Immunology, Medical University of Vienna, Vienna 1090, Austria

CD19 chimeric antigen receptor T (CD19CAR-T) cells have achieved promising outcomes in relapsed/refractory B cell malignancies. However, recurrences occur due to the loss of CAR-T cell persistence. We developed dual T/B cell co-stimulatory molecules (CD28 and CD40) in CAR-T cells to enhance intense tumoricidal activity and persistence. CD19.28.40z CAR-T cells promoted pNF-κB and pRelB downstream signaling while diminishing NFAT signaling upon antigen exposure. CD19.28.40z CAR-T cells demonstrated greater proliferation, which translated into effective anti-tumor cytotoxicity in long-term co-culture assay. Repetitive weekly antigen stimulation unveiled continuous CAR-T cell expansion while preserving central memory T cell subset and lower expression of exhaustion phenotypes. The intrinsic genes underlying CD19.28.40z CAR-T cell responses were compared with conventional CARs and demonstrated the up-regulated genes associated with T cell proliferation and memory as well as down-regulated genes related to apoptosis, exhaustion, and glycolysis pathway. Enrichment of genes toward T cell stemness, particularly SELL, IL-7r, TCF7, and KLF2, was observed. Effective and continuing anti-tumor cytotoxicity in vivo was exhibited in both B cell lymphoblastic leukemia and B cell non-Hodgkin lymphoma xenograft models while demonstrating persistent T cell memory signatures. The functional enhancement of CD37.28.40z CAR-T cell activities against CD37⁺ tumor cells was further validated. The modification of dual T/B cell signaling molecules remarkably maximized the efficacy of CAR-T cell therapy.

INTRODUCTION

Adoptive immunotherapy with specific chimeric antigen receptor T cell (CAR-T) is a synthetic receptor that redirects T lymphocytes to recognize and eradicate certain tumor cells expressing the cognate antigen.[1] The US Food and Drug Administration-approved CD19CAR-T cells that incorporate either CD28 or 4-1BB as a co-stimulatory domain displayed remarkable clinical outcomes in B cell hematologic malignancies. Complete remission rates were demonstrated in 70%–90% in relapsed/refractory acute B cell lymphoblastic leukemia (B-ALL) patients who had poor outcomes with conventional therapy.[2–6] A moderate to complete remission range of 20%–70% was reported in B cell non-Hodgkin lymphoma (B-NHL) and chronic lymphocytic leukemia.[7–11] Although CD19CAR-T cells have achieved initial high response rates, recurrence following therapy still occurs due to poor CAR-T persistence.[2–7] Various approaches have been widely studied to improve CAR-T cell functions including intracellular signal domain modifications. The intracellular domain typically consists of one or more co-stimulatory domains mediating favorable T cell activation and persistence, and a major T cell activating motif, the zeta subunit of CD3 complex (CD3ζ).[12]

The activation of nuclear factor-κB (NF-κB) plays a significant role in promoting CAR-T cell longevity and tumoricidal activity[13] such that downstream signaling exists in both T and B cells upon stimulation.[14–18] NF-κB signaling is divided into two major pathways: canonical and non-canonical, which are different from stimuli, response, and biological functions. For example, the canonical pathway by T cell receptor (TCR) and CD28 co-stimulatory domain (TCR/CD28) stimulation results in rapid and transient signaling. CD40, which is a member of the tumor necrosis factor receptor (TNFR) family expressed widely on B cells, triggers non-canonical pathways contributing to slow but persistent NF-κB.[19,20] A study by Zhao et al. revealed that CD19CAR-T cells incorporating CD28 co-stimulatory domain of T cells rapidly eradicated tumor cells in a xenograft model. However, another 4-1BB co-stimulatory domain reflected slower but persistent cytotoxicity owing to similar tumor control. They incorporated CD28 and 4-1BBL into CD19CAR-T cells to sustain superior tumoricidal activity that enhanced

interferon-beta/interferon regulatory factor 7 activation and conferred more efficient cytotoxicity.[21] Furthermore, Julamanee et al. developed a B cell signaling moiety, CD79A/CD40, compositing CD19CAR-T cells (CD19.79a.40z) that demonstrated strong NF-κB and nuclear factor of activated T cells (NFAT) upon antigen stimulation and promoted greater CAR-T cell proliferation and cytotoxicity. However, the kinetics of T cell cytotoxicity in the early phase of CD19.79a.40z CAR-T cells were slower than CD19.28z CARs.[22]

To maximize CAR-T cell efficacy, we hypothesized that a combination of T and B cell signaling molecules CD28 and CD40 (CD28.40z) would synergize both canonical and non-canonical NF-κB signaling as well as enhance both intense tumoricidal activity and T cell persistence, which are required for CAR-T cell therapy. We investigated the functional enhancement of CD28/CD40 co-stimulatory domain using third-generation CD19CAR-T and CD37CAR-T cells against B cell malignancies.

RESULTS

CD28/CD40 co-stimulatory domain mediated NF-κB signaling while diminishing the NFAT signaling pathway in a CD19CAR model

We developed CD19CAR that incorporated CD28/CD40 co-stimulatory domain (CD19.28.40z) to examine synergistic signals contributed by the dual T/B cell co-stimulatory domain CD28/CD40 in CAR-T cells. Second-generation CD19CAR with either CD28 (CD19.28z), 4-1BB (CD19.BBz), or CD40 (CD19.40z) co-stimulatory domain were parallel modified and used as the control CAR (Figure 1A). We generated CD19CAR-T cells as described in Figure 1B. The CD19CAR-T cells were successfully introduced into primary human CD3+ cells with similar transduction efficiency (range, 38.0%–66.9%) and were enriched to greater than 92% purity (range, 92.4%–98.2%) after purification (Figures 1C and 1D). To verify the similar expression of CAR and truncated human epidermal growth factor receptor (tEGFR), we stained CAR-T cells with anti-CD19CAR FMC63 together with anti-EGFR that CD19CAR-T cells equally expressed both EGFR and CD19CAR FMC63 in all structures (Figures 1E and 1F). The tEGFR+ mean fluorescence intensity (MFI) was further assessed to confirm the homogeneous and consistent expression of CARs in multiple donors. At pre-selection, CD19.28z CAR-T cells showed the lowest tEGFR+ MFI followed by CD19.28.40z CAR-T cells. However, there were no significant differences of tEGFR+ MFI among CAR-T constructs after tEGFR selection (Figure S1A). Expanding with CD19+-specific stimulation by EBV-LCL feeder cells, CD19.28.40z CAR-T and CD19.BBz CAR-T cells showed significantly increased fold expansion compared with CD19.28z CAR-T or CD19.40z CAR-T cells (Figure S1B). CAR-T cells stimulated with anti-CD3/CD28 beads revealed similar proliferation among CAR constructs.

We performed intracellular phospho-flow analysis to evaluate the downstream T cell signaling alteration upon CD19 engagement.

CD19.28.40z CAR-T cells exhibited a significantly higher phospho-NF-κB and a trend of phospho-RelB at baseline; however, CD19.BBz CAR-T and CD19.40z CAR-T cells in turn elevated phospho-NF-κB and phospho-RelB after activation (Figure 1G). Moreover, both CD19.28.40z CAR-T and CD19.28z CAR-T cells enhanced phospho-ZAP-70 upon antigen stimulation, which was not seen early on in CD19CAR-T cells incorporated with TNFR family domains (Figure S2A). Likewise, CD19.BBz CAR-T and CD19.28.40z CAR-T cells slightly increased phospho-p38 signaling while no statistically significant difference in phospho-ERK was observed among CAR constructs (Figure S2A). We further confirmed provisional downstream signals of the CD28/CD40 co-stimulatory domain incorporating CD19CAR-T at the transcriptional level using CAR-transduced Jurkat-Triple parameter reporter (TPR) cells in which the activity of NFAT and NF-κB were simultaneously measured.[23,24] CD19.28z CAR-transduced Jurkat-TPR cells significantly activated tonic NFAT signaling without antigen stimulation (Figures 1H and S2B). Upon CD19 antigen stimulation, CD19.28.40z CAR-T cells generated a low level of NFAT activity. However, CD19.40z CAR-T cells produced less NF-κB activity compared with other co-stimulatory domains (Figures 1H and S2B). In addition, the levels of NFAT and NF-κB signaling were slightly enhanced in CD19.28.40z CAR-T cells following K562 (CD19-negative) stimulation compared with the others (Figure S2B). Together, we successfully generated CD19CAR-T cells and incorporated CD28/CD40 co-stimulatory domain, which promoted high NF-κB downstream signal transduction and less produced NFAT signaling upon CD19-specific stimulation.

Prominent CAR-T cell proliferation and endogenous interleukin-2 secretion of CD19.28.40z CAR-T cells conferred superior anti-tumor efficacy

The CD28/CD40 signaling domain was assessed to determine whether or not it could enhance CD19CAR-T cell proliferation after stimulation with CD19 antigen. CD19CAR-T cells were stimulated once with CD19+ target cells and cultured in medium supplemented with or without interleukin-2 (IL-2). Particularly, a greater fold expansion of CAR-T cells was observed in CD19.28.40z CAR-T cells regardless of cytokine supplementation compared with other CAR constructs (Figure 2A). The notable differences in proliferation were statistically significant after culturing for 6 and 8 days as well as lasting until the end of culture without and with exogenous IL-2, respectively. Next, we sought to determine the differences in cytokine production and secretion among CAR structures. Using intracellular cytokine staining assay, CD19.28z CAR-T and CD19.28.40z CAR-T cells statistically produced higher proportion of IL-2 compared with CD19.BBz CAR-T and CD19.40z CAR-T cells after a short incubation time with CD19+ antigen. Moreover, the sustained high level of IL-2 secretion by CD19.28.40z CAR-T cells was demonstrated after overnight incubation compared with other structures. On the other hand, CD19.28z CAR-T cells showed a tendency to have higher percentage of interferon-γ (IFN-γ) production after short and long incubation times (Figure 2B).
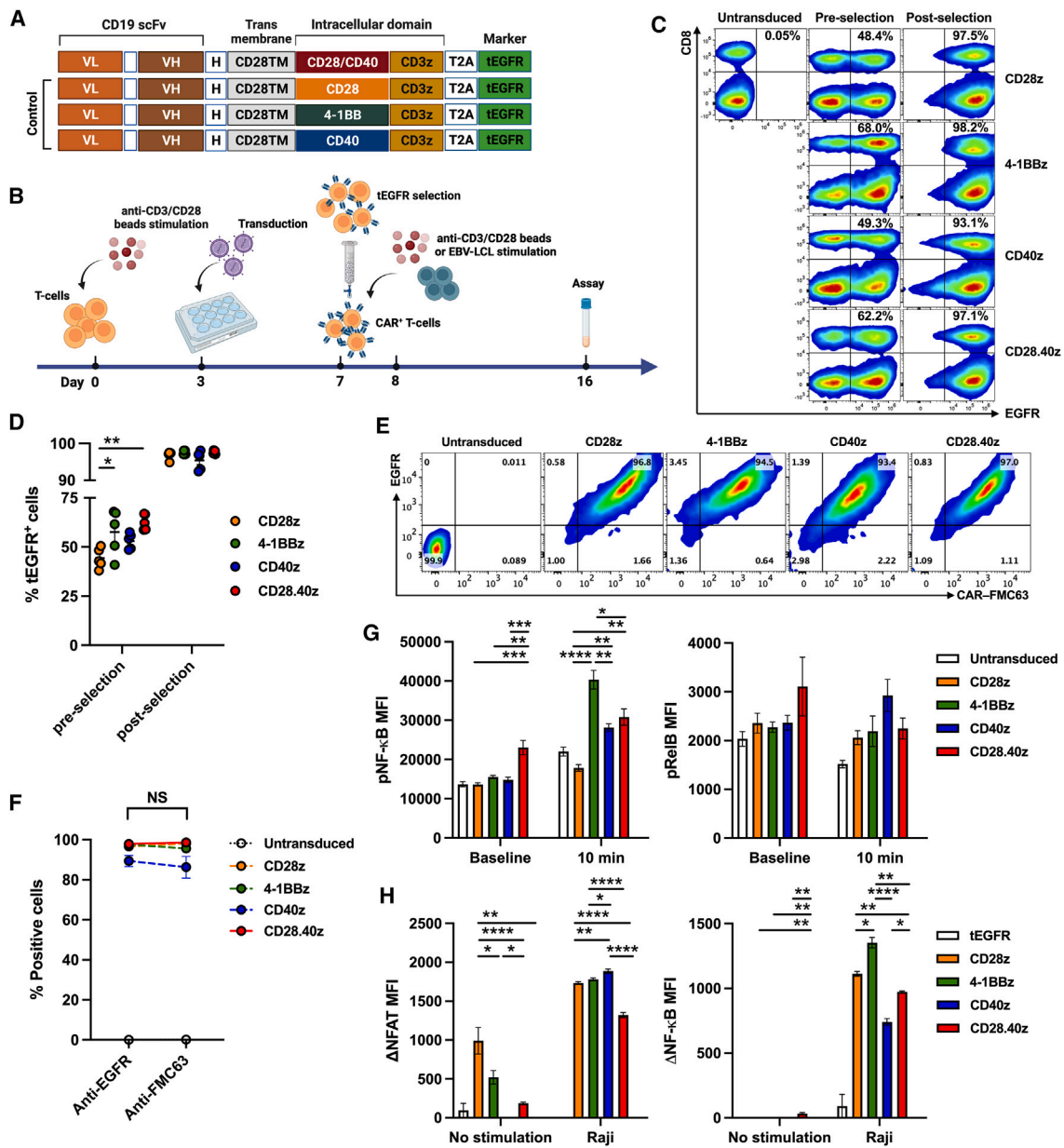
Figure 1. CD19CAR-T cell generation and T cell signaling assay

(A) Schematic of CD19CAR constructs. The intracellular domain of CD28/CD40 (CD28.40z), CD28 (CD28z), 4-1BB (BBz), or CD40 (CD40z) was fused into the anti-CD19CAR backbone; CD19 scFv-H-CD28TM-IC-CD3ζ-tEGFR. scFv, single chain variable fragment; VL, light-chain variable fragment; VH, heavy chain variable fragment; H, short 12 amino acid of IgG4 Fc-derived spacer of hinge; TM, transmembrane domain; IC, intracellular domain; tEGFR, truncated EGFR. (B) Schematic of CD19CAR-T cell generation. EBV-LCL; EBV-transformed lymphoblastoid cell line. (C) Representative flow plots of transduced primary human T cells stained for tEGFR expression after 7 days of activation at pre- and post-selection. (D) Transduction efficacy and purification of CD19CAR-T cells from five different donors. The data are presented as mean ± SEM. One-way ANOVA; $*p < .05$, $**p < .01$. (E) Representative flow plots of untransduced-T and purified CD19CAR-T cells stained for EGFR and CD19CAR FMC63 expressions. (F) EGFR and CD19CAR FMC63 expressions of T cells. Data were pooled from three different donors and presented as mean ± SEM. Student's t test; p = ns. (G) Mean fluorescence intensity (MFI) data of intracellular phospho-specific staining of pNF-κB (left) and pRelB (right). Untransduced- or CD19CAR-T cells were stimulated with CD19-K562 cells at an E:T ratio of 1:5 for 10 min. Data were collected from three different donors and are presented as mean ± SEM. (H) Activation of ΔNFAT (left) and ΔNF-κB (right) MFI using Jurkat-triple parameter reporter (TPR) cells transduced with different CAR structures. tEGFR-transduced or CD19CAR-transduced Jurkat-TPR cells were stimulated with Raji cells at a 1:1 ratio for 24 h. The activation of NFAT and NF-κB was measured using flow cytometry. The MFI of ΔNFAT or ΔNF-κB was calculated as the difference between each datum and the mean of stimulated/untransduced Jurkat-TPR cells. Triplicate assays were performed. Data are presented as mean ± SEM. One-way ANOVA for (D), (G), and (H); $*p < .05$, $**p < .01$, $***p < .001$, $****p < .0001$.
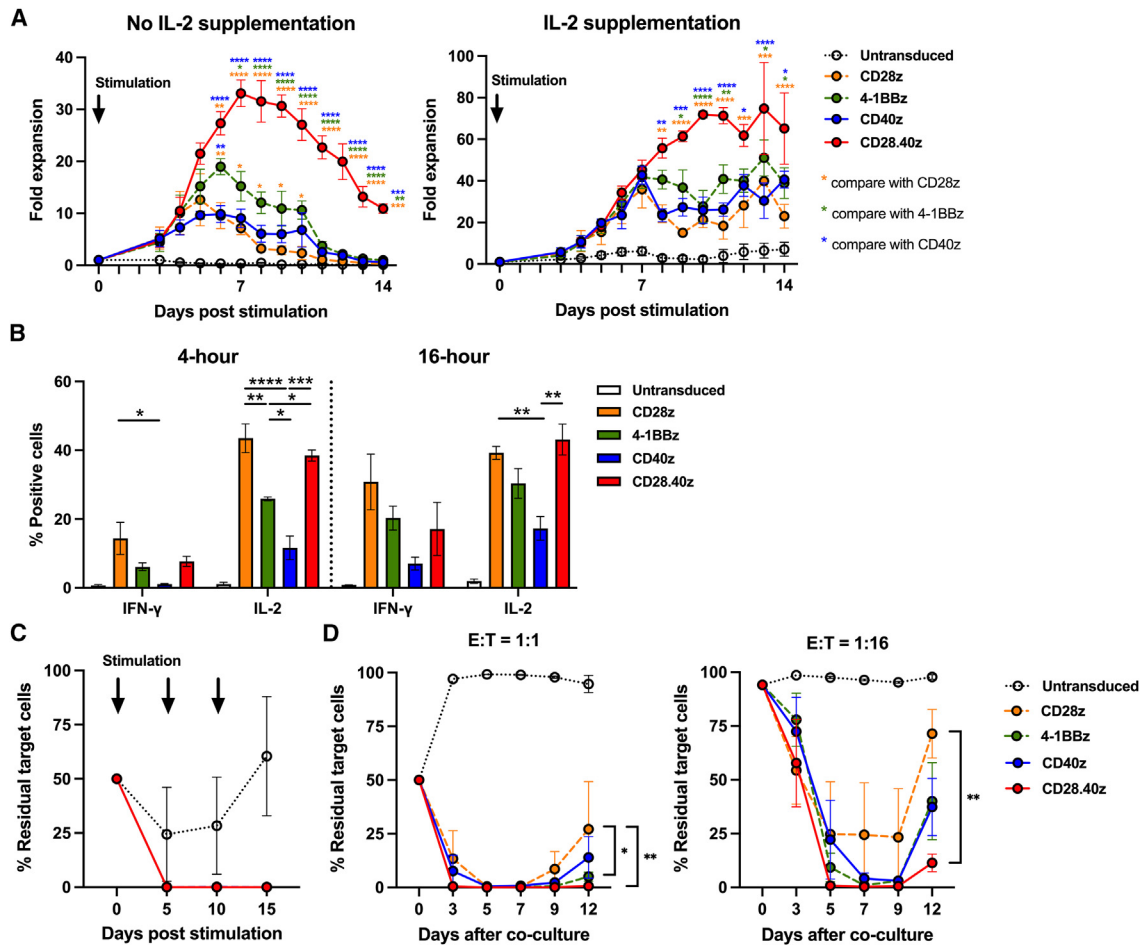
Figure 2. CD19CAR T cell proliferation, cytokine secretion upon antigen stimulation and cytotoxicity

(A) T cell proliferation assay. Untransduced- or CD19CAR-T cells were stimulated with γ-irradiated CD19-K562 cells at a 1:1 ratio. The cultures were divided into two conditions: without (left) or with (right) IL-2 supplementation (50 IU/mL). The proliferation of T cells was assessed by counting viable cells for 14 days. Arrows mark the day of being stimulated with CD19-K562 cells. (B) Intracellular cytokine staining for IFN-γ and IL-2. T cells were stimulated with CD19-K562 cells at an E:T ratio of 1:2 for 4 h and 16 h, permeabilized, and stained for intracellular IFN-γ and IL-2. (C) Repetitive target cell stimulation assay. Untransduced- or CD19CAR-T cells were cultured with NALM-6 at an E:T ratio of 1:1 every 5 days for three consecutive stimulations with IL-2 supplementation. Flow cytometry was used at the designated time points to evaluate the proportions of effector and residual tumor cells. (D) Prolonged co-culture assay. Untransduced- or CD19CAR-T cells were co-cultured with NALM-6/ffluc-GFP at E:T ratios of 1:1 (left) and 1:16 (right) for a total of 12 days without IL-2 supplementation. Flow cytometry was used at the designated time points to evaluate the proportions of effector and residual tumor cells. All data were pooled from three different donors and are presented as mean ± SEM. Two-way ANOVA for (A), (C), and (D); one-way ANOVA for (B); $*p < .05$, $**p < .01$, $***p < .001$, $****p < .0001$.

To assess the cytotoxic activity of CD19CAR-T cells following repetitive target cell stimulation *in vitro*, we cultured T cells with fresh NALM-6 cells at a 1:1 ratio every 5 days for three consecutive stimulations and cultured with IL-2 supplementation. The cultured cells were analyzed for effector function by flow cytometry, and all CAR-T cell constructs showed complete tumor cell eradication on day 5, 10, and 15, compared with control-T cells (Figure 2C). We further examined whether the superior proliferative capacity and higher endogenous IL-2 secretion of CD19.28.40z CAR-T cells would contribute to the improvement of anti-tumor activity. CAR-T cells were cultured long-term with CD19+ target cells at various effector-to-target (E:T) cell ratios without IL-2 supplementation and assessed for the percentage of effector T cells as well as residual target cells using flow cytometry at the indicated time points. Remarkably, CD19.28.40z CAR-T cells continued to eliminate the tumor cells until the last day of the experiment at all E:T ratios, whereas the tumor cells began to recur in other constructs at the end of the assay (Figures 2D and S1C). To define the mechanism of tumor recurrence, we checked CD19 antigen expression on the residual NALM-6 cells at the last date of long-term co-culture assay. The result showed a trend of higher percentage of residual CD19 antigen-negative NALM-6 cells in lower E:T ratios without any difference among CAR structures (Figure S1D). These results indicated that greater proliferation and persistence of CD19.28.40z CAR-T cells would enhance tumoricidal activity.
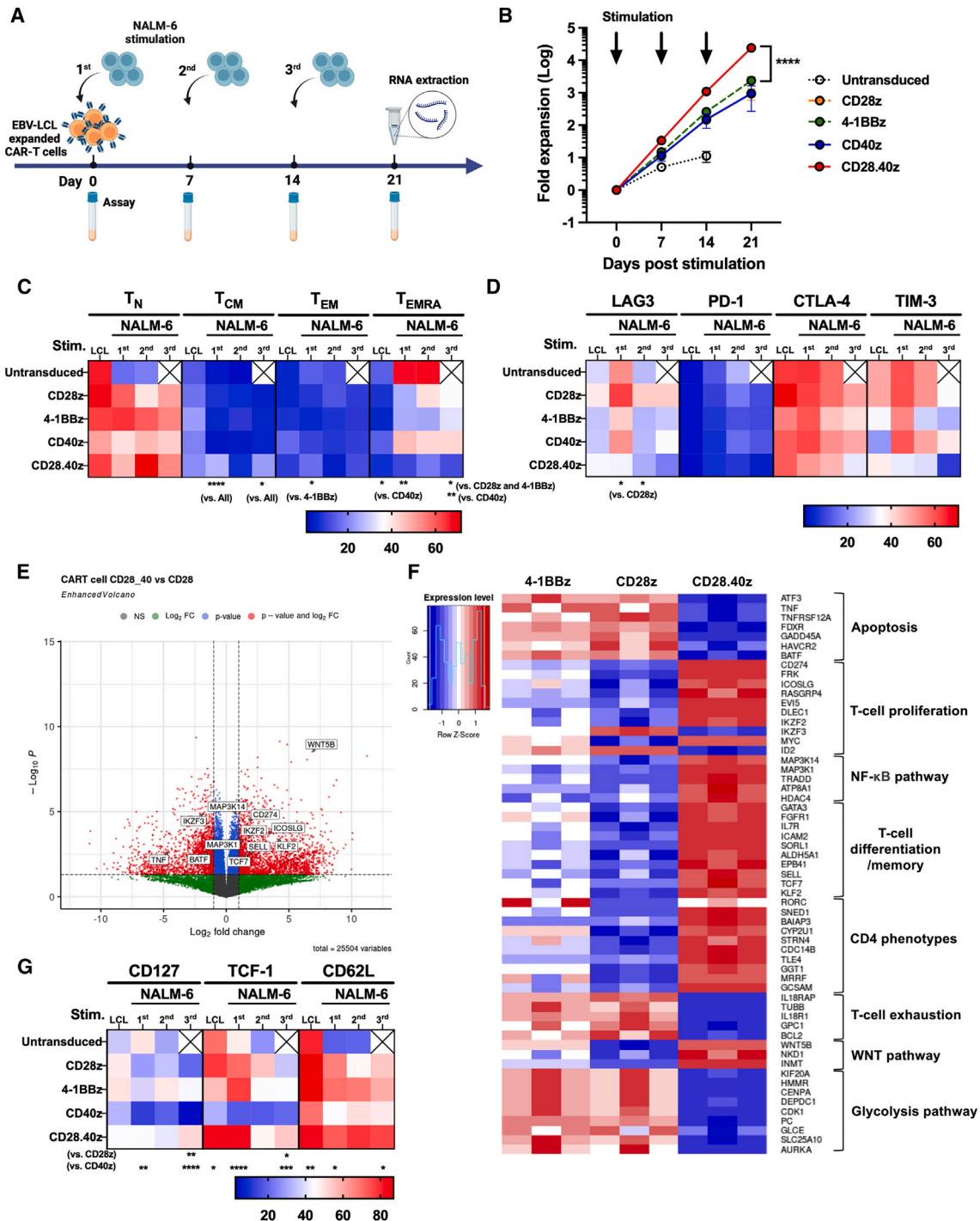
Figure 3. CD19CAR-T immunophenotype assays and differential gene expression profiling analyses

(A) Schematic of chronic antigen stimulation and immunophenotype assays. Untransduced- or EBV-LCL-expanded CD19CAR-T cells were stimulated weekly with γ-irradiated NALM-6 cells at a 1:1 ratio for 3 consecutive weeks and cultured with IL-2 supplementation (50 IU/mL). Expansion of CD19CAR, T cell differentiation, and exhaustion phenotypes were then evaluated before and after weekly stimulation. On day 21, the remaining CD19CAR-T cells, 3×10^6 cells, were harvested and extracted for RNA. (B) Fold expansion of T cells after chronic antigen stimulation. T cell expansion was measured by counting viable cells. Arrows mark the day of NALM-6 cell stimulation. (C and D) Heatmap of T cell immunophenotype assays. (C) T cell differentiation subset heatmap to assess the percentage of CD62L$^+$ CD45RA$^+$ naive T (T$_N$), CD62L$^+$ CD45RA$^-$ central memory T (T$_{CM}$), CD62L$^-$ CD45RA$^-$ effector memory T (T$_{EM}$), and CD62L$^-$ CD45RA$^+$ effector memory re-expressing CD45RA T (T$_{EMRA}$) cells before and

(legend continued on next page)

CD19.28.40z CAR-T cells sustained higher CAR-T proliferation without influencing T cell fate and exhaustion following repetitive stimulation

We conducted repetitive weekly antigen stimulation and assessed the dynamic changes in T cell proliferative capacity as well as the T cell differentiation and exhaustion immunophenotypes of CAR-T cells to mimic persistent antigen stimulation as *in vivo*. CD19CAR-T cells underwent three consecutive weekly stimulations with γ-irradiated NALM-6 cells at a 1:1 ratio and were cultured with IL-2 supplementation. Differences in T cell expansion, T cell subset, and exhaustion phenotypes at pre- and post-stimulation among CD19CAR-T constructs were assessed at indicated time points (Figure 3A). CD19.28.40z CAR-T cells continually proliferated with remarkable fold expansion after repetitive stimulation compared with the others (Figure 3B). Next, we examined the dynamic alteration in T cell differentiation by staining T cells with CD45RA and CD62L along with classification into CD45RA$^+$CD62L$^+$ naive T, CD45RA$^-$CD62L$^+$ central memory T (T$_{CM}$), CD45RA$^-$CD62L$^-$ effector memory T (T$_{EM}$), and CD45RA$^+$CD62L$^-$ effector memory re-expressing CD45RA T (T$_{EMRA}$) cell subsets. Following multiple stimulations, a significant positive T$_{CM}$ and a small number of T$_{EMRA}$ populations in CD19.28.40z CAR-T cells were noticed among other co-stimulatory domains (Figure 3C). We further explored the impact of CD4:CD8 T cell ratios on a CAR-T cell subset following repetitive antigen stimulation. All CAR structures showed the CD4:CD8 T cell ratios of 1:2 before antigen stimulation; however, those ratios were mostly converted into all CD8$^+$ T cell populations after repeated antigen encounters without significant differences among CAR constructs (Figure S3A). Additionally, the T cell exhaustion phenotypes, including PD-1, CTLA-4, TIM-3, and LAG3, tended to be less expressed in CD19.28.40z CAR-T cells (Figure 3D). These results underlined the superior CAR-T cell proliferation with preservation of less-differentiated T cell subsets of CD19.28.40z CAR-T cells following repetitive antigen encounters.

## CD28/CD40 incorporated CD19CAR-T cells enriched genes toward T cell stemness

We further investigated the mechanism underlying the advantages of CD28/CD40 signaling molecules over conventional T cell co-stimulatory domains. Regarding CD40 co-stimulation, the initial *in vitro* functions showed the inferior CAR-T cell functions compared with CD19.28.40z CAR, we therefore did not further assess the transcriptional profiles and *in vivo* function of this structure. CD19CAR-T cells at the end of the chronic antigen stimulation assay were harvested and extracted for ribonucleic acid (RNA). The transcriptomic differences among CAR constructs were then determined using RNA sequencing (Figure 3A). Differentially expressed genes (DEGs) were assessed between two group comparisons (i.e., CD19.28.40z vs. CD19.28z, and CD19.28.40z vs. CD19.BBz CAR-T cells). The distributions of all DEGs obtained from each comparison with some of the significantly expressed genes related to CAR-T cell functions are shown in volcano plots (Figures 3E and S3D). The statistical significance of the DEG data (adjusted *p* value) vs. magnitude of expression change (log2fold change) is also shown. The results highlighted the significantly up-regulated genes associated with T cell proliferation including *ICOSLG*, *RASGRP4*, *EVI5*, *DLEC1*, and *IKZF2*, and T cell differentiation and memory-related genes, which include *GATA3*, *FGFR1*, *IL7R*, *SELL*, *TCF7*, and *KLF2*, in CD19.28.40z CAR-T cells compared with CD28 or 4-1BB co-stimulatory domains. Moreover, NF-κB pathway, wingless-type (Wnt) pathway, and CD4+ phenotype-associated genes were also enriched in CD19.28.40z CAR-T cells, in contrast, the genes related to apoptosis, exhaustion, and glycolysis pathways were down-regulated (Figure 3F). In relation to memory gene signatures, we noticed the enrichment of specific genes toward T cell stemness namely *SELL, IL-7r, TCF7,* and *KLF2* in CD19.28.40z CAR-T compared with conventional CAR-T cells (Figure 3F). We investigated the corresponding degrees of CD127, TCF-1, and CD62L expression over time following a chronic antigen stimulation assay to validate stemness expression by CD19.28.40z CAR-T cells. Interestingly, CD19.28.40z CAR-T cells continually expressed higher levels of CD127$^+$, TCF-1$^+$, and CD62L$^+$ over time after stimulation compared with other CAR-T structures (Figures 3G and S3C). Moreover, the molecular pathway using gene set enrichment analysis (GSEA) to interpret the genome-wide transcriptional profiles related to CAR-T function upon antigen stimulation demonstrated that CD19.28.40z CAR-T cells enriched in genes related to memory and fatty acid metabolism compared with CD19.28z CAR-T or CD19.BBz CAR-T cells (Figure S3E). Consequently, the stemness gene signatures of CD19.28.40z CAR-T cells conferred advantages in CAR-T expansion and persistence following repetitive antigen stimulation.

CD19.28.40z CAR-T cells mediated effective tumor clearance in a B-ALL murine model

We assessed the CD28/CD40 co-stimulatory domain to determine if it effectively affected the *in vivo* cytotoxicity of CD19CAR-T cells against B-ALL. NALM-6-bearing NOD-scid common-γ chain knockout (NSG) mice were treated with a low CD19CAR-T cell dose to assess the efficacy and functional limits of CAR-T therapy (Figure 4A). CD19.28.40z CAR-T cells effectively suppressed tumor

---

after stimulation over time. (D) T cell exhaustion heatmap to evaluate the percentage of LAG3$^+$, PD-1$^+$, CTLA-4$^+$, and TIM-3$^+$ T cells before and after stimulation over time. Data were pooled from three different donors and are shown as mean ± SEM; two-way ANOVA for (B); one-way ANOVA for (C) and (D); *p < .05, **p < .01, ****p < .0001. (E) Volcano plot of DEGs between CD19.28.40z CAR-T vs. CD19.28z CAR-T cells. Visualization of DEGs in a volcano plot. The red marks represent up-regulated and down-regulated genes with false discovery rate (FDR) < 0.05. DEGs were identified using criteria of FDR ≤0.05 and ≥2.0-fold difference. (F) Heatmap of normalized RNA sequencing reads, under the indicated CD19CAR-T cells in various gene categories related to T cell functions. Gene names are presented on the right side and each CAR construct was marked at the top of the colored map. The color bar provides a visual representation of the normalized count values. (G) Heatmap of the percentages of CD127$^+$, TCF-1$^+$, and CD62L$^+$ T cells stimulated as in (A), before and after stimulation over time. Data were pooled from three different donors and are shown as mean ± SEM; one-way ANOVA; *p < .05, **p < .01, ***p < .001, ****p < .0001.
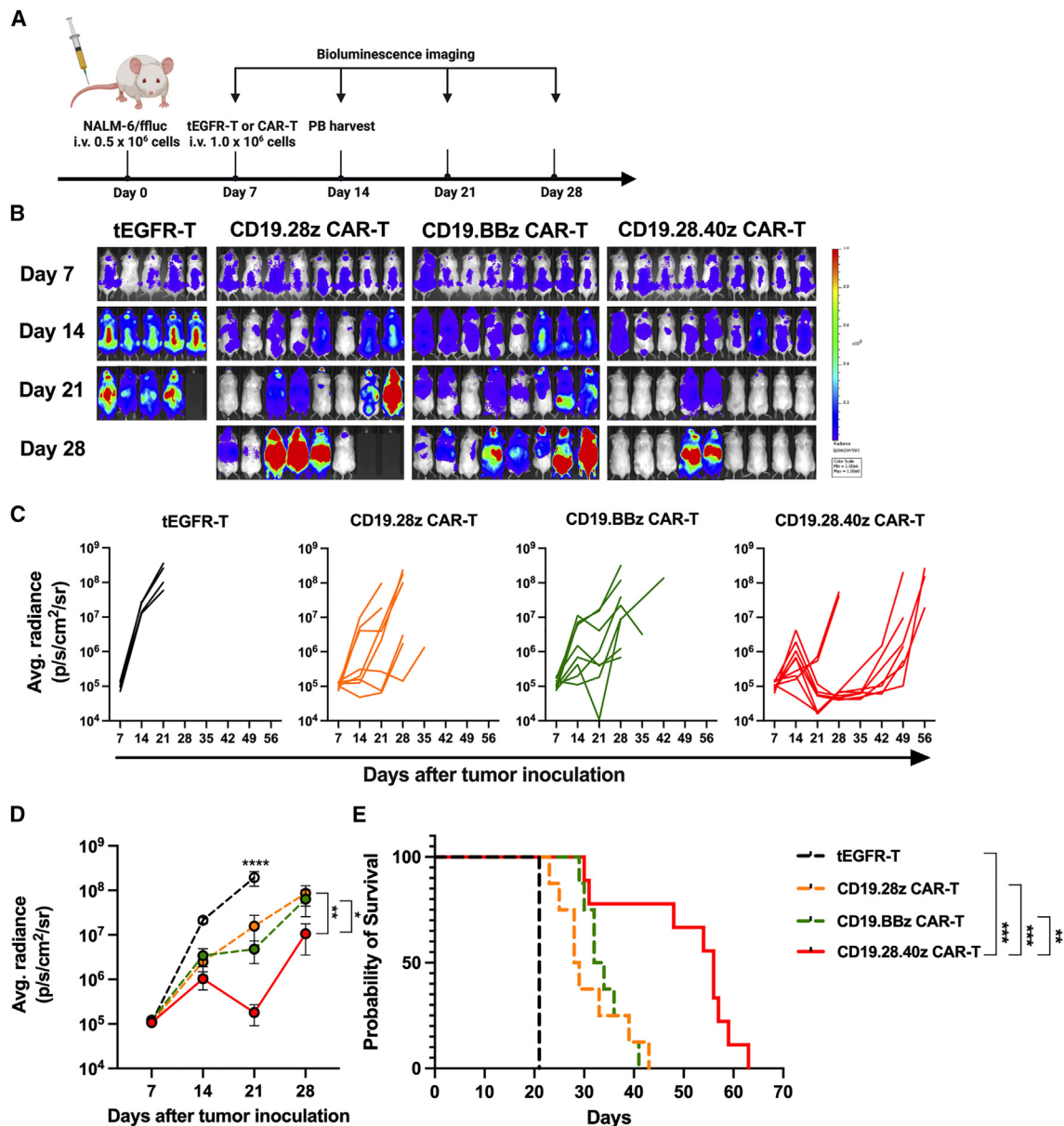
Figure 4. *In vivo* CD19CAR-T mediated tumor clearance in B-ALL murine model

(A) Schematic of the *in vivo* experiments. NOD-SCID common-γ chain knockout (NSG) mice were inoculated with 0.5×10^6 NALM-6/fluc-GFP cells via the tail vein injection on day 0. Then, either 1×10^6 tEGFR-T or CD19CAR-T cells were injected on day 7. Tumor burden was assessed using bioluminescence imaging (BLI) at the indicated time points. (B) Representative BLI of NALM-6-inoculated mice treated with control or CD19CAR-T cells over time. (C) Tumor burden of individual mice treated with tEGFR-, CD19.28z CAR-, CD19.BBz CAR-, or CD19.28.40z CAR-T cells over time was calculated and reported as average radiance, which was the sum of the radiance from each pixel inside the region of interest divided by the number of pixels or super pixels. (D) Summarized tumor burden of mice treated with control-T or CD19CAR-T cells at indicated time points. Data are presented as mean ± SEM and summarized from three independent experiments using three different donors (CD19CAR-T cells: $n = 8$–9 per group; tEGFR-T: $n = 5$); two-way ANOVA; $^*p < .05$, $^{**}p < .01$, $^{****}p < .0001$. (E) Kaplan-Meier analysis of survival of NALM-6/fluc-bearing NSG mice (Log rank [Mantel-Cox] test; $^{**}p < .01$, $^{***}p < .001$).

cell growth compared with the control arms (Figure 4B). In terms of tumor-killing kinetics, we observed a rapid and uniformly sustainable tumor suppression of average radiance in mice treated with CD19.28.40z CAR-T cells that resulted in a remarkable improvement in overall survival (Figures 4B–4E). Meanwhile, CD19.28z CAR-T and CD19.BBz CAR-T cells showed non-uniform and ineffective tumor suppression leading to short-term survival (Figures 4C–4E). Moreover, we evaluated the presence of human CD3$^+$ cells in the
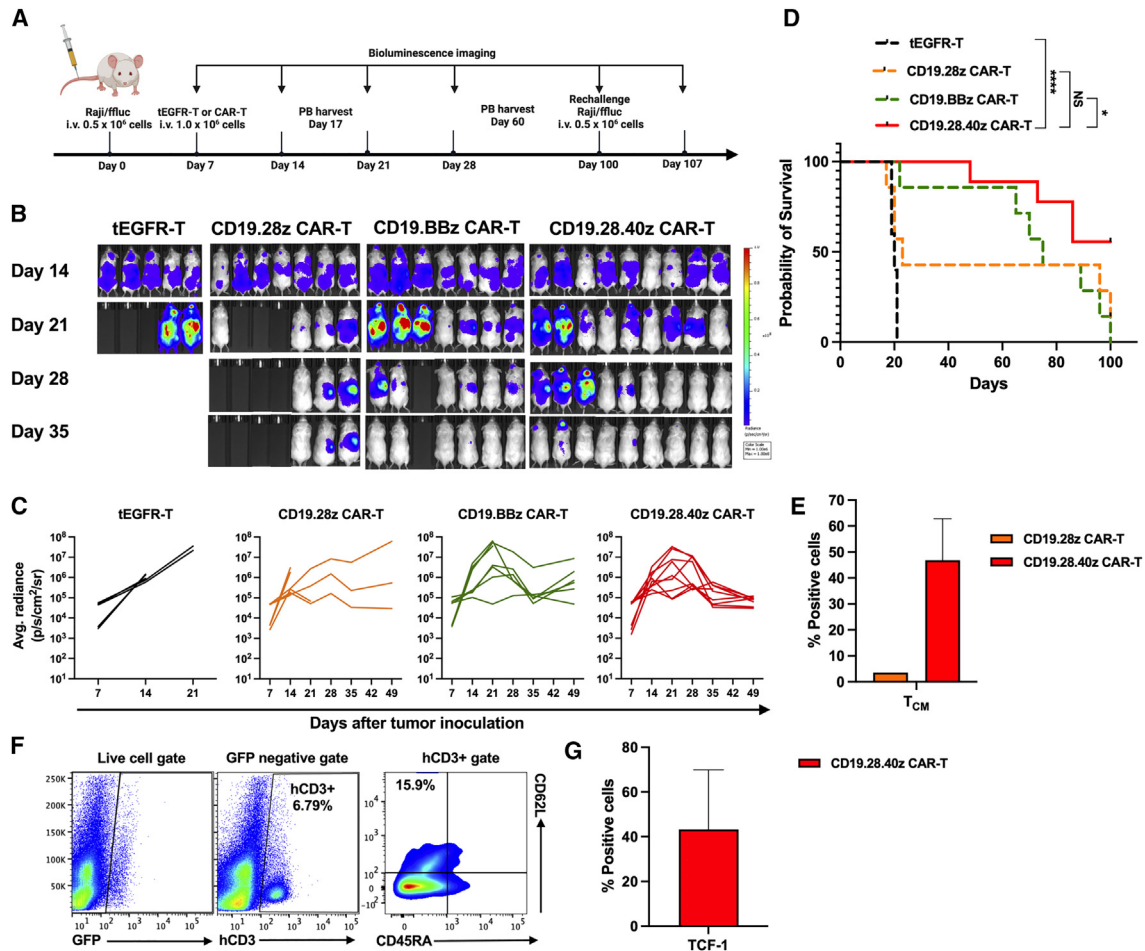
Figure 5. Memory signatures of *in vivo* CD19CAR-T conferred persistent tumor control in B-NHL murine model

(A) Schematic of the *in vivo* experiments. On day 0, NSG mice were inoculated with 0.5×10^6 Raji/ffluc-GFP cells via tail vein injection. Then, either 1×10^6 tEGFR-T or CD19CAR-T cells were injected on day 7. The surviving mice were re-challenged with 0.5×10^6 Raji/ffluc-GFP cells via tail vein injection on day 100. Tumor burden was assessed using bioluminescence imaging (BLI) at the indicated time points. (B) Representative BLI of Raji-inoculated mice treated with control- or CD19CAR-T cells over time. (C) Tumor burden of individual mice treated with tEGFR-, CD19.28z CAR-, CD19.BBz CAR-, or CD19.28.40z CAR-T cells over time was calculated and reported as average radiance, which was the sum of the radiance from each pixel inside the region of interest divided by the number of pixels or super pixels. Data are presented as mean ± SEM and summarized from three independent experiments using three different donors (CD19CAR-T cells: $n = 7$–9 per group; tEGFR-T: $n = 5$). (D) Kaplan-Meier analysis of survival of Raji/ffluc-bearing NSG mice (Log rank [Mantel-Cox] test; $p = $ ns, $*p < .05$, $****p < .0001$). (E) Percentage of human CD62L$^+$ CD45RA$^-$ central memory T (T_{CM}) cells from peripheral blood collected on day 100 (CD19.28z CAR-T: $n = 1$; CD19.28.40z CAR-T: $n = 4$) from surviving mice. (F) Representative flow plots of human CD3$^+$ cells and T cell differentiation phenotypes and (G) Percentage of TCF-1$^+$/CD3$^+$ cells in bone marrow on day 150 from euthanized mice receiving CD19.28.40z CAR-T cells (CD19.28.40z CAR: $n = 2$).

peripheral blood of the mice 7 days after the T cell transfer. However, no significant differences among the CAR-T constructs were observed in the circulating human CD3$^+$ cells (Figure S4A). We initially monitored the body weights of the mice to determine whether the CAR-T co-stimulatory domains influenced cytokine release syndrome. We found that the mice treated with CD19.28.40z CAR-T cells maintained consistent weight throughout the observation period, while the mice in the control groups experienced weight loss (Figure S4B). Additionally, the mice serum concentrations of IFN-γ and IL-6 showed insignificant differences among CAR-T structures after T cell transfer for 7 days (Figure S4C). In summary, CD19.28.40z

CAR-T cells effectively eradicated B-ALL and prolonged survival in the murine model.

Memory signature of CD19.28.40z CAR-T persistently eradicated B-NHL tumor *in vivo*

We conducted an additional study using a Raji-bearing NSG mouse model with administration of a low dose of CAR-T cells (Figure 5A). Similar to the previous B-ALL murine model, superior tumoricidal activity and uniform eradication kinetics were observed in CD19.28.40 CAR-T cells (Figures 5B and 5C), which translated into significantly prolonged overall survival at day 100 compared with

tEGFR-T and CD19.BBz CAR-T cells (Figure 5D). We again identified insignificant differences of circulating human CD3$^+$ cells in the peripheral blood of the mice on days 10, 60, and 100 after adoptive T cell transfer among treatment arms (Figure S5A). Alternatively, we deliberately defined the immunological memory characteristic of the T cell central memory subset in the peripheral blood of the mice on day 100. The result indicated a median T$_{CM}$ population of 46.8% in mice treated with CD19.28.40z CAR-T compared with less than 5% in the CD19.28z CAR-T group (Figures 5E and S5B). The cured mice were re-challenged with a Raji-ffluc cell line on day 100 and followed for an additional 50 days to further investigate the *in vivo* effectiveness, persistence, and establishment of compelling long-term memory signatures (Figure 5A). A bioluminescence analysis revealed noticeable tumor progression in CD19.28z CAR-T cell-treated mice. However, the mice that received CD19.28.40z CAR-T experienced long-term tumor control until the end of the experiment (Figures S5C and S5D). The surviving mice treated with CD19.28.40z CAR-T were eventually euthanized on day 150. The bone marrow exhibited persistent human CD3$^+$ cells, which were mainly central and effector memory T cells (Figure 5F) as well as preserved TCF-1 positive cells substantiating the formation of long-term memory stemness in the lymphoma xenograft model (Figure 5G). In particular, greater infiltration of CD19.28.40z CAR-T cells was demonstrated in the bone marrow, liver, and spleen (Figure S5E). The body weights and serum IFN-γ and IL-6 of the mice were monitored and found to be comparable to those in the previous B-ALL model (Figures S5F and S5G). From these findings, we confirmed that the memory signature of CD19CAR-T that incorporated CD28/CD40 signaling molecules, translating into effective and sustainable tumor killing in the xenograft models.

CD37.28.40z CAR-T cells confirmed the functional enhancement of the co-stimulatory domain

The anti-CD37CAR-T cells that incorporated CD28/CD40 were parallelly generated to confirm the feasibility of the co-stimulatory domain. The second-generation CD37CAR-T cells with either CD28 (CD37.28z), or 4-1BB (CD37.BBz) co-stimulatory domains were used as control arms (Figure 6A). We successfully generated CD37CAR-T cells with a transduction efficacy of 46.2%–76.6% and a purification of 94.0%–99.3% (Figure 6B). CD37CAR-T cell proliferation was first assessed by stimulation with CD37$^+$ target cells and cultured without exogenous IL-2, which again demonstrated a robust proliferation compared with other controls (Figure 6C). We further assessed T cell subsets and found that CD37.28.40z CAR-T cells were mostly CD4$^+$ population at baseline compared with other structures. After co-culturing with CD37$^+$ target cells, all CD37CAR-T constructs were predominantly expressed CD8$^+$ cells except the CD37.28z CAR-T that showed a higher percentage of CD4$^+$ cells (Figure S6A). For T cell phenotypes, CD37.28.40z CAR-T and CD37.BBz CAR-T cells preserved the naive T cell phenotype compared with CD37.28z CAR-T cells upon antigen exposure (Figure 6D). Notably, the significantly low levels of LAG3$^+$ and PD-1$^+$ cells were observed in CD37.28.40z CAR-T cells compared with other structures at the end of culture (Figure 6E). Furthermore, CD37.28.40z CAR-T cells effec-

tively suppressed tumor cell growth in a long-term culture assay at an E:T cell ratio of 1:1 without exogenous IL-2, whereas tumor outgrowth was observed early on in other CAR constructs (Figure 6F). These findings validated the functional enhancement of CD28/CD40 signaling molecules in CD37CAR-T cells that resulted in superior T cell proliferation and tumoricidal activity against CD37-positive tumor cells.

The sequence of CD28 and CD40 co-stimulatory molecules in CAR structure affects CAR-T cell functions

The previous experiments demonstrated the superior CD19.28.40z CAR-T cell functions compared with control CAR-T cells. These functional advantages resemble CD19.28z CAR-T function more than CD19.40z CAR-T cells. We therefore hypothesized that the sequence of CD28 upstream to CD40 molecules may contribute to the greater CAR-T cell functions. To examine whether the sequence of CD28 and CD40 co-stimulatory molecules in CAR structure would affect CAR-T cell function, we generated a CD19.40.28z CAR construct to directly compare with CD19.28.40z CAR (Figure S7A). The lower transduction efficacy and purification of CD19.40.28z CAR-T cells compared with CD19.28.40z CAR-T cells were observed (Figures S7B and S7C). Moreover, CD19.40.28z CAR-T cells demonstrated significantly lower CAR-T cell expansion after being stimulated with CD19$^+$ target cells with or without exogenous IL-2 compared with CD28/CD40 co-stimulatory domain (Figures S7D and S7E). For the T cell subset, the naive T cell phenotype was predominantly expressed by CD19.40.28z CAR-T; in contrast, CD19.28.40z CAR-T robustly expressed T$_{CM}$ at baseline. Following CD19$^+$ antigen stimulation, CD19.40.28z CAR-T cells had lower LAG3$^+$ cells, whereas insignificant differences in the T cell subset among CAR-T constructs were observed (Figures S7F and S7G). In terms of cytokine secretion, CD19.28.40z CAR-T statistically produced a higher proportion of IFN-γ and IL-2 compared with CD19.40.28z CAR-T cells after short and overnight incubations with CD19$^+$ antigen (Figure S7H). Moreover, CD19.28.40z CAR-T cells effectively suppressed tumor cell growth in a long-term culture assay at an E:T cell ratio of 1:8 without exogenous IL-2 compared with CD19.40.28z CAR-T cells (Figure S7I). In summary, the sequence modification by incorporating CD40 upstream to CD28 co-stimulatory molecules dampened the CAR-T cell proliferation, cytokine secretion, and target cell cytotoxicity compared with the CD28/CD40 co-stimulatory domain. These results corroborated the hypothesis that the sequence of CD28 and CD40 co-stimulatory molecules in CAR structure affects CAR-T cell functions.

DISCUSSION

The current clinical experiences involving CD19CAR-T cells in adults with relapsed/refractory B-ALL and B-NHL demonstrated suboptimal outcomes. The persistence of CAR-T in patients has been found to be correlated with clinical benefit.[25] In this study, we aimed to investigate the impact of an innovative dual T/B cell signaling domain (i.e., CD28/CD40) on the effectiveness of both CD19CAR-T and CD37CAR-T therapy against B cell hematologic malignancies.
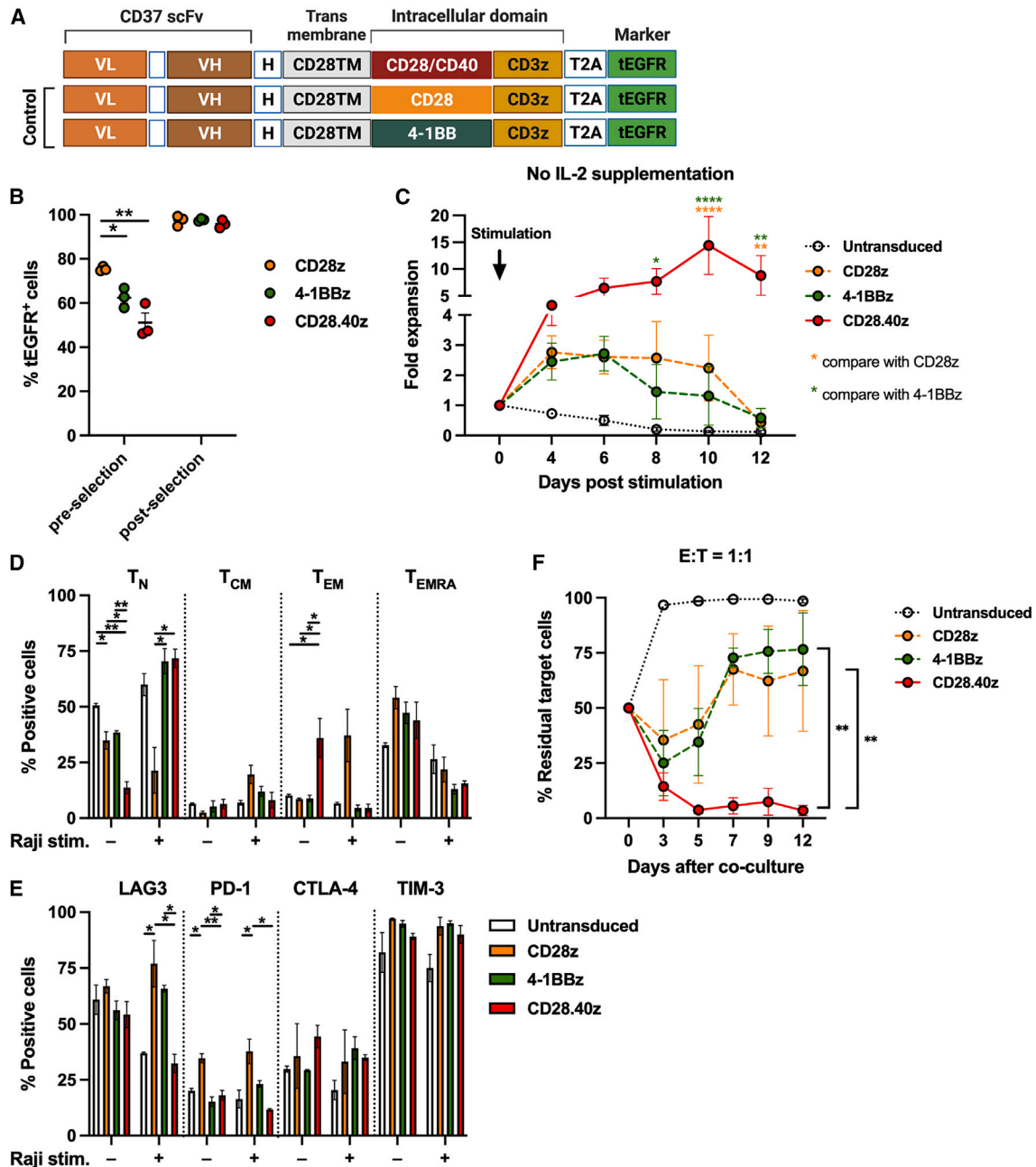
Figure 6. Generation and *in vitro* assays of CD37CAR-T cells

(A) Schematic of CD37CAR constructs. The intracellular domain of CD28/CD40 (CD28.40z), CD28 (CD28z), or 4-1BB (BBz) was fused into the anti-CD37CAR backbone; CD37 scFv-H-CD28TM-IC-CD3ζ-tEGFR. scFv, single chain variable fragment; VL, light-chain variable fragment; VH, heavy chain variable fragment; H, short 15 amino acid of IgG1 Fc-derived spacer of hinge; TM, transmembrane domain; IC, intracellular domain; tEGFR, truncated EGFR. (B) Transduction efficiency and purification of CD37CAR-T cells. (C) T cell proliferation assay. Untransduced- or CD37CAR-T cells were stimulated with γ-irradiated Raji cells at E:T ratio of 1:2 and cultured without IL-2 supplementation for 12 days. T cell proliferation was measured by counting viable cells. Arrows mark the day of being stimulated with the target cells. (D) Percentage of T cell differentiation subset of CD62L$^+$ CD45RA$^+$ naive T (T$_N$), CD62L$^+$ CD45RA$^-$ central memory T (T$_{CM}$), CD62L$^-$ CD45RA$^-$ effector memory T (T$_{EM}$), and CD62L$^-$ CD45RA$^+$ effector memory re-expressing CD45RA T (T$_{EMRA}$) cells before and after Raji cell stimulated as in (C). (E) Percentage of T cell exhaustion of LAG3$^+$, PD-1$^+$, CTLA-4$^+$, and TIM-3$^+$ T cells before and after Raji cell stimulated as in (C). (F) Prolonged co-culture assay. Untransduced- or CD37CAR-T cells were co-cultured with Raji/ffluc at a 1:1 ratio without IL-2 supplementation for a total of 12 days. The percentages of effector and residual target cells were assessed by flow cytometry at the indicated time points. All data were pooled from two to three different donors and are presented as mean ± SEM. One-way ANOVA for (B), (D), and (E); two-way ANOVA for (C) and (F); *$p < .05$, **$p < .01$, ***$p < .001$, ****$p < .0001$).

We initially hypothesized that a combination of CD28 and CD40 co-stimulatory domains would potentiate NF-κB, which is a key regulator in immune responses, proliferation, differentiation, and cell survival.[26] The downstream signaling of NF-κB is present in both T and B cells, thereby contributing to stronger CAR-T functions. The CD28 co-stimulatory receptor on T cells stimulates the canonical NF-κB signal, which leads to a rapid and transient function. However, CD40 expressed widely on B cells triggers a non-canonical pathway that contributes to slower but persistent NF-κB activation.[20] According to our experimental results, incorporating CD28/CD40 into the CD19CAR backbone synergized the baseline non-canonical and canonical NF-κB signaling compared with the control CD28, 4-1BB, or CD40 co-stimulatory domains. Additionally, CD19.28.40z-transduced Jurkat-TPR cells confirmed the increment of basal NF-κB with significantly less NFAT activity after stimulation with Raji. However, this effect could not be observed after co-culturing with CD19-K562. Philipson et al. demonstrated that conventional CD19.BBz CAR-T exhibited longer persistence than CD19.28z CAR-T due to basal NF-κB signaling and further enhancement following antigen engagement of non-canonical NF-κB.[27] In the context of CAR-T cell therapy, excessive levels of NFAT, which is a transcription factor involved in the regulation of T cell activation and differentiation, drive T cell exhaustion and reduce its efficacy.[28–30] A study by Munroe et al. showed the co-stimulatory function of CD40 in T cells that both mouse- and human-hCD40+ T cell lines had a tendency of higher NFAT, AP-1, and NF-κB signaling following anti-CD3/CD28/CD40 stimulation.[18] Another study investigated the role of combined activation of the NFAT and NF-κB pathways during TCR or CAR signaling in human T cells and found that both signals could physically co-bind to the same cis-regulatory regions that regulate essential T cell response genes.[31] To the best of our knowledge, there is little evidence of NFAT and NF-κB signaling crosstalk in CAR-T cells to clarify the reduction of NFAT in our study. These findings should be validated in the upcoming TCR-T or CAR-T cell studies to further elucidate the mechanism of this phenomenon. Collectively, basal enhancement of NF-κB signaling by the CD28/CD40 co-stimulatory domain and the reduction of NFAT activity conferred advantages for T cell proliferation and persistence.

As a proof of concept, CD19.28.40z CAR-T cells displayed strong and sustained T cell expansion after co-culturing with CD19⁺ target cells, which contributed to the superior tumoricidal activity in the long-term co-culture assay. Regarding the highly preserved T_N population among CAR-T constructs in this study, the plausible factor would be the condition of cell culture that CAR-T cells were stimulated with an irradiated cell line as the feeder cells and supplemented with IL-2. The chronic antigen stimulation assay additionally confirmed the greater and continuing CAR-T proliferation and preservation of T cell stemness and fewer exhaustion phenotypes. Fewer differentiated characteristics, such as those seen in our findings, were shown to influence engraftment, expansion, longevity, and superior tumoricidal activity, which contributed to greater CAR-T efficiency against B cell malignancies.[32] Interestingly, we observed the near identical *in vitro* functions of CD19.40z CAR-T and CD19.BBz CAR-T cells in terms of

T cell proliferation and cytotoxicity. Similar to a recent study by Levin-Piaeda et al. in which they investigated the second- and third-generation anti-human leukocyte antigen (HLA)-A2 CAR endowed CD40 co-stimulatory domain and found the comparable T cell signaling and cytokine secretion mediating target cell killing among CD40 and 4-1BB co-stimulations.[33] These findings emphasize the class effect of non-canonical NF-κB pathway activation by CD40 or 4-1BB co-stimulatory molecule in T cells.

RNA sequencing was performed to assess the CAR-T intrinsic gene alteration following repetitive antigen stimulation. The DEGs exhibited significantly up-regulated genes associated with T cell proliferation and memory, NF-κB pathway, Wnt pathway, and CD4+ phenotypes in CD19.28.40z CAR-T cells. The enrichment of T cell stemness genes, including *SELL, IL-7r, TCF7,* and *KLF2* as well as a diminishing of the *ID2* transcription factor, in the dual T/B cell signaling domain were identified. The higher corresponding levels of CD127, TCF-1, and CD62L protein expression were additionally validated in CD19.28.40z CAR-T cells following multiple stimulations. In CAR-T cell therapy, the presence of memory T cell signatures desirably provides long-lasting protection against cancer. In particular, the maintenance of stem-like T cells by TCF-1, which is encoded by *TCF7*, is an essential transcription factor of the canonical Wnt signaling pathway. It also allows the transcription of memory-related genes such as *CCR7, IL7Ra (CD127), SELL (CD62L),* and *CXCR5*.[34] In addition, the activity of TCF-1 is inhibited by *ID2*. In the murine chronic viral infection models, the absence of *ID2* substantiated the elevation of stem-like precursors.[35,36] Moreover, we indicated a decline in the expression of genes involved in apoptosis, exhaustion, and the glycolysis pathway in CD19.28.40z CAR-T compared with conventional CAR-T. Some considerably down-regulated genes (e.g., *IKZF3* and *BATF*) in CD19.28.40z CAR-T were translated into greater functioning of CAR-T cells. Zou et al. demonstrated that the inactivation of the *IKZF3* gene, which is in the Ikaros Zinc Finger (IkZF) transcription factor family, was involved in immune cell development and cytokine signaling. *IKZF3* gene inactivation promoted proliferation of CAR-T cells and improved anti-tumor activity in solid tumors in both *in vitro* and xenograft models.[37] Furthermore, the depletion of basic leucine zipper ATF-like transcription factor enhanced CAR-T anti-tumor efficacy by influencing resistance to exhaustion and the formation of central memory T cells.[38] Metabolic pathways, such as glycolysis and fatty acid oxidation, are crucial for T cell programming, which provides the necessary energy and biosynthetic precursors to support T cell differentiation.[39] According to a previous study, the specific metabolic mechanisms utilized by CAR-T cells were correlated with memory generation. In particular, CD28-based CD19CAR-T cells depended on glycolytic metabolism that resulted in the development of an effector memory population. Meanwhile, 4-1BB-endowed CD19CAR-T cells had a greater reliance on fatty acid metabolism contributing to central memory formation.[40,41] Concomitantly, GSEA demonstrated that CD19.28.40z CAR-T cells enriched in fatty acid metabolism-related genes compared with conventional CAR constructs.

The aforementioned advantages allowed CD19.28.40z CAR-T cells to significantly reduce tumor cell growth in both B-ALL- and B-NHL-inoculated mice over several weeks that resulted in remarkable long-term survival. Zhao et al. examined tumor-killing kinetics among CAR designs by conducting a study to investigate distinctive tumor-killing features between conventional CD19.28z and CD19.BBz CAR-T cells in a xenograft model. CD19.28z CAR-T cells exhibited strong and rapid anti-tumor activity, whereas CD19.BBz CAR-T cells revealed gradual and persistent tumor elimination.[21] The underlying mechanisms of CAR-T cell activity together with the natural history of diseases are responsible for the observed outcomes. B-ALL is a rapid-growing and aggressive type of cancer that involves the blood and bone marrow while B-NHL is a slow developing cancer that primarily affects lymph nodes.[42] Thus, the *in vitro* robust T cell proliferation and persistent anti-tumor cytotoxicity exhibited by CD19.28.40z CAR-T cells translated into potent tumoricidal activity, hindrance of tumor recurrence, and ultimately improved overall survival in the NALM-6 inoculated mice model. In contrast, CD19.28z and CD19.BBz CAR-T cells displayed non-uniform and ineffective tumor killing that resulted in early tumor relapse and dismal survival outcomes. Although there were no differences among circulating CAR-T cell constructs at different time points, the evidence of long-term persistence as well as the retaining of T cell stemness signatures of CD19.28.40z CAR-T cells *in vivo* were denoted, even after tumor rechallenge. The additional assessment for *in vivo* T cell expansion through flux imaging may be needed in the future study.

We further examined the feasibility of incorporating CD28/CD40 into CD37CAR-T cells.[43] CD37.28.40z CAR-T cells were engineered and confirmed remarkable proliferation as well as tumoricidal activity against CD37-positive malignancies compared with CD28 or 4-1BB co-stimulatory domain. In addition, CD37.28.40z CAR-T cells also preserved the naive T cell phenotype and expressed the low level of exhaustion markers following antigen exposure similar to the CD19CAR model. Levin-Piaeda et al. investigated the third-generation HLA-A2 CAR incorporated CD28/CD40 or CD28/4-1BB co-stimulatory domain and found that both CARs similarly transduced NFAT signaling, while CD28/4-1BB endowed CAR demonstrated lower NF-κB signaling after stimulation with HLA-A2^{+} target cells. Moreover, CAR-T cells that incorporated CD28/CD40 signaling molecules significantly produced higher levels of IFN-γ, IL-2, and TNF-α concentration upon exposure to target cells.[33] Hence, the functional advantages of the co-stimulatory domain (i.e., CD28/CD40) were validated.

Furthermore, we also investigated whether the sequence of CD28 and CD40 molecules on CAR structure would affect CAR-T cell functions. Compared with CD28/CD40 co-stimulatory domain, CD19CAR incorporated with CD40 upstream to CD28 co-stimulatory molecules demonstrated the inferior CAR-T cell functions. The mechanism that could account for the differences is the distance of the signaling molecule to the cytoplasmic membrane. A study by Guedan et al. revealed that the membrane proximity of ICOS to 4-1BB co-stimulatory domains of anti-mesothelin CAR-T cells displayed a dominant effect over the distal domain.[44] In addition, the study by Si et al. also demonstrated that the distance of signaling molecule to the cytoplasmic membrane is important for CAR functions of the synthetic co-signaling modules of the immunoglobulin-like superfamily and TNFR superfamily.[45] These results emphasize the crucial role of the proximal-distal location of co-stimulatory molecules in CAR structure.

This study has a few limitations. First, we did not compare CAR-T cells endowed CD28/CD40 co-stimulation with other third-generation CARs that incorporated the established dual CD28/4-1BB, MyD88/CD40, or CD79A/CD40 co-stimulatory domains which were beyond our scope of this current research. Moreover, the *in vivo* function of CD37CAR incorporated CD28/CD40 co-stimulatory domain was not done in this study. The further CD28/CD40 endowed CAR-T cell models are needed to corroborate the superior co-stimulatory function of the dual T /B cell signaling molecules.

In summary, the dual T/B cell signaling domain of CD28/CD40 enhanced basal NF-κB signaling and memory signatures that potentiated CD19CAR-T cell proliferation and persistence. The result was greater anti-tumor efficacy in both *in vitro* and xenograft models. The simplified structural modification of the signaling molecule is favorable for maximizing the functionality and stemness of CAR-T cells.

MATERIALS AND METHODS
Cell lines
Our laboratory maintains the NALM-6, Raji, and K562 cell lines. CD19-K562 cell lines were generated by retrovirally transducing K562 cells to express truncated CD19 antigen, as described elsewhere.[46] NALM-6 and Raji cells were lentivirally transduced to express green fluorescent protein (GFP) and firefly luciferase (ffluc), which were established elsewhere.[22,43] The CD19^{+} Epstein-Barr virus-transformed lymphoblastoid cell line (EBV-LCL) was employed as a feeder for CAR-T cells. Cell lines were cultured in RPMI-1640 (Gibco, Life Technologies Corp., CA, USA) supplemented with 10% fetal bovine serum, 1% penicillin-streptomycin, and 0.8 mM L-glutamine.

Viral vector construction
The CD19CAR single chain variable fragment (scFV) construct in this study was based on the FMC63 clone.[47] Various co-stimulatory domains, including CD28/CD40 (CD28.40z), CD40/CD28 (CD40.28z), CD28 (CD28z), 4-1BB (BBz), or CD40 (CD40z), were incorporated into the anti-CD19CAR scFv-IgG4/hinge-CD28 transmembrane domain followed by the CD3ζ intracellular domain. The CD28/CD40 or CD40/CD28 co-stimulatory domain was synthesized by connecting CD28 amino acid position 180–220 (GenBank: J02988) to CD40 amino acid position 216–277(GenBank: NM_001783) with a GGG amino acid linker. In addition, the CD37CAR structure including anti-CD37 scFv based on the CAS-024 clone (VL – linker – VH) – IgG1 hinge – CD28TM – CD28IC – CD3ζ IC was used as a template to generate CD37CAR structures that incorporated the

4-1BB or CD28/CD40 co-stimulatory domain.[43] All CAR constructs were fused with a self-cleaving T2A sequence and a truncated epidermal growth factor receptor (tEGFR) as a surface marker for CAR expression at equimolar levels from a single transcript that was previously established.[22,48,49] CAR genes were then inserted into the LZRS-pBMN-Z vector, and the sequences were confirmed by direct sequencing. Gammaretroviral supernatants were generated using the Phoenix-Ampho system (Orbigen, San Diego, CA, USA).

Generation of CAR-T cells

Peripheral blood mononuclear cells were isolated from the whole blood of healthy donors by density-gradient centrifugation using Lymphoprep (STEMCELL Technologies Inc., Canada). Anti-human CD3 immunomagnetic beads (Miltenyi Biotec, Bergisch Gladbach, Germany) were used to purify CD3$^+$ cells, which were subsequently activated using anti-CD3/CD28 beads (Invitrogen, Carlsbad, CA, USA). On day 3, retroviral transduction was conducted using a recombinant human retronectin fragment-coated plate (Retronectin, Takara Bio, Otsu, Japan), followed by centrifugation at 2100 rpm for 1 h at 32°C. The transduced T cells were cultured in RPMI 1640 (Gibco, Life Technologies Corp., CA, USA) medium containing 10% human serum, 0.8 mM L-glutamine, 1% penicillin-streptomycin, and 0.5 μM 2-mercaptoethanol (cytotoxic T cell medium; CTL) and supplemented with 50 IU/mL recombinant human interleukin-2 (IL-2). On day 7, CAR$^+$ T cells were selectively enriched using biotin-conjugated monoclonal antibodies (mAb) against EGFR and anti-biotin beads (Miltenyi Biotec). The purified CAR$^+$ T cells were expanded by co-culturing with either γ-irradiated EBV-LCL feeder cells at a 1:7 T cell:feeder cell ratio or anti-CD3/CD28 beads at a 1:1 ratio for 8–10 days before further use or freeze down. Untransduced-T cells were cultured along with the transduced T cells except for the viral addition. The frozen cells were thawed under 37°C in bath warmer and rested in CTL medium with IL-2 supplementation overnight before use.

Transcription factor and T cell signaling assay

Jurkat-triple parameter reporter (TPR) cells, which responded to the effects of co-stimulatory domains on NF-κB, NFAT, and AP-1 signal transduction and drove the expression of fluorescent proteins CFP, eGFP, and mCherry collectively, were used in the experiment.[23,24] Jurkat-TPR cells were transduced with CD19CAR genes and purified to express greater than 95%. Then, untransduced- or CD19CAR-transduced Jurkat-TPR cells were co-cultured with γ-irradiated K562, CD19-K562, or Raji cells at a 1:1 E:T ratio for 24 h and analyzed using flow cytometry. Regarding the lack of appropriate laser detection in our institute, AP-1 activity (mCherry) could not be evaluated. Furthermore, intracellular phospho-flow analysis was performed to assess downstream signaling upon CAR-T activation. Untransduced- or CD19CAR-T cells were mixed with CD19-K562 cells at an E:T ratio of 1:5 for 10 min. Then, the cells were fixed with 2% formaldehyde at 37°C for 10 min, permeabilized with cold 90% methanol, and incubated on ice for 30 min. Phospho-specific antibodies, including phospho-ZAP-70, phospho-p38, phospho-p44/42 MAPK (ERK1/2), phospho-NF-κB p65, and phospho-RelB

rabbit mAb (Cell Signaling Technology, Danvers, MA, USA), were used for primary staining and donkey anti-rabbit IgG (BioLegend) as secondary antibody.

Proliferation assay

Untransduced- or CAR-T cells were stimulated with γ-irradiated CD19-K562 or Raji cells at a 1:1 ratio and cultured without or with IL-2 supplementation. Viable cell counting was determined using trypan blue agent from day 3 until the last day of the experiment.

Repetitive target cell stimulation assay

Untransduced- or CAR-T cells were cultured with NALM-6 at an E:T ratio of 1:1 every 5 days for three consecutive stimulations with exogenous IL-2 supplementation. Flow cytometry was used at designated time points to evaluate the proportions of effector and residual tumor cells.

Long-term co-culture assay

Untransduced- or CAR-T cells were co-cultured with NALM-6/ffluc-GFP or Raji/ffluc-GFP at E:T ratios of 1:1, 1:4, 1:8, and 1:16 for up to 12 days without exogenous IL-2 to examine CAR-T cell cytotoxicity as well as the proliferative capacity. Flow cytometry was used at designated time points to evaluate the proportions of effector and residual tumor cells.

Intracellular cytokine staining assay

Untransduced or CD19CAR-T cells were stimulated with CD19-K562 cells at an E:T ratio of 1:2 for 4 h and 16 h, then fixed and permeabilized with a fixation/permeabilization kit (BD Biosciences). The stimulated cells were stained for intracellular IFN-γ and IL-2.

Immunophenotypes

All samples were analyzed by CytoFLEX S (Beckman Coulter, CA, USA) or FACSAria Fusion (BD Biosciences, NJ, USA) flow cytometers. The FlowJo software (Tree Star, OR, USA) was used for data analyses. The monoclonal antibody-conjugated fluorophores were stained in the experiments (all lists are shown in Table S1): CD3; CD8; CD45RA; CD62L; PD-1; TIM-3; IFN-γ; IL-2 (BD Biosciences); mCD45; CTLA-4; LAG3; CD127, and TCF-1 (BioLegend); CD19CAR FMC63 (Miltenyi Biotec).

Chronic antigen stimulation assay

T cells were weekly stimulated with γ-irradiated NALM-6 cells at a 1:1 ratio for 3 consecutive weeks and cultured with exogenous IL-2. Then, the T cell expansion, T cell subsets, T cell exhaustion, and T cell stemness phenotypes were assessed at pre-stimulation and post-stimulation on days 0, 7, 14, and 21. At post-stimulation on day 21, the remaining CD19CAR-T cells 3–5 × 10^6 cells were harvested and extracted for RNA.

RNA sequencing, differential gene expression, and GSEA

The RNA Blood Mini Kit (QIAGEN GmBH, Germany) was used to extract RNA. A total of nine RNA samples from three independent healthy donors with RNA integrity number score >7 were used to

undergo polyA selection and TruSeq RNA library preparation (TruSeq Stranded mRNA LT Kit; Illumina). Samples were barcoded and analyzed on a Hiseq 4000 Illumina platform. The quality control of the raw sequence read data in the FASTQ file was evaluated using the FastQC tool. The Trimmomatic tool trimmed the adapters and contaminating sequences and short sequence reads were mapped to the reference genome from GENCODE (GRCh38) to identify the position using HISAT2. The reads were then assembled using Stringtie software to reconstruct the full-length transcript. The expression count matrix was computed using Stringtie software. The differentially expressed genes (DEGs) were selected at a false discovery rate (FDR) ≤ 0.05 and a fold change ≥ 2.0-fold difference using the EdgeR program. The EnhancedVolcano and Heatmap packages in R version 4.1.2 were used to create volcano plots and heatmaps depicting DEGs. The gene set enrichment analysis (GSEA) was performed using software version 4.2.3 to identify the enriched pathways. Published gene sets of ontology (MsigDB) were used for the analysis. The enrichment plot was considered statistically significant with a nominal p value $\leq .05$ and an FDR q value ≤ 0.25.

Acute B-lymphoblastic leukemia and Burkitt's lymphoma xenograft models

Six- to 8-week-old male NOD-SCID common-γ chain knockout (NSG) mice were intravenously inoculated with 0.5×10^6 NALM-6/ffluc or Raji/ffluc cells via the tail vein. Control tEGFR-transduced or CD19CAR-T 1×10^6 cells were intravenously injected a week later. For the rechallenge protocol, 0.5×10^6 Raji/ffluc cells were re-injected via the tail vein on day 100 in surviving mice. Mice were subjected to perform weekly bioluminescence imaging (Caliper Life Science, Waltham, MA, USA) to assess tumor progression. Quantification was done by measuring the average radiance and baselines, and subsequent body weights were monitored. Mouse survival was assessed based on death as the endpoint. Peripheral blood was obtained via the tail vein on days 7, 10, 60, or 100 after the T cell transfer. Erythrocyte lysis buffer (QIAGEN GmBH, Hilden, Germany) was used to remove the erythrocytes, and then the resting leukocytes were analyzed by flow cytometry. Mouse sera were collected on day 7 or day 10 and measured for IFN-γ and IL-6 concentrations using an enzyme-linked immunosorbent assay (BD Biosciences). Subsequently, the surviving mice were euthanized on day 150. The livers, spleens, bone marrow, and peripheral blood were excised and drawn to assess CAR-T cell persistence, T cell memory signatures, and residual tumor cells.

Statistical analysis

The statistical analysis was conducted using Prism 9.5.1 software (GraphPad Software, La Jolla, CA, USA). The experimental data were presented as mean ± SEM. Differences among the results were assessed using Student's t test, one-way ANOVA, or two-way ANOVA with appropriate Bonferroni or Tukey posttest corrections. Survival times were analyzed using the Kaplan-Meier method and evaluated through a Log rank (Mantel-Cox) test. Statistical significance was determined when the p value was <.05.

Study approval

The experiment study was approved by the Human Research Ethics Committee of the Faculty of Medicine, Prince of Songkla University, Thailand (REC.63-262-14-1). All human samples were collected from healthy donors who provided written informed consent following the principles outlined in the Declaration of Helsinki. All murine experiments were approved by the Institutional Animal Care and Use Committee of Prince of Songkla University (Project license number 2564-02-072 ref. 80/2021).

DATA AND CODE AVAILABILITY

The datasets presented in this study can be found in online repositories: NCBI under accession ID PRJNA994608 (https://www.ncbi.nlm.nih.gov/bioproject/?term=PRJNA994608).

SUPPLEMENTAL INFORMATION

Supplemental information can be found online at https://doi.org/10.1016/j.omton.2024.200837.

AUTHOR CONTRIBUTIONS

Conception and design: W.K., P.C., S.T., and J.J. Development of methodology: W.K., P.C., S.T., and J.J. Acquisition of data: W.K., P.C., N.J., K.M., S.U., S.T., and J.J. Analysis and interpretation of data (e.g., statistical analysis, computational analysis): W.K., P.C., and J.J. Writing, review, and/or revision of the manuscript: W.K., P.C., S.O., S.S., P.V., P.S., S.T., and J.J. Administrative, technical, or material support (e.g., reporting or organizing data, constructing databases): W.K., P.C., S.S., P.V., P.S., J.L., S.O., S.T., and J.J. Study supervision; S.S, S.T, and J.J.

DECLARATION OF INTERESTS

W.K., N.J., P.V., S.T., and J.J. are the inventors of patent applications for CD28/CD40 Co-Stimulatory Domain of The Chimeric Antigen Receptor, submitted by Prince of Songkla University, Songkhla, Thailand. S.O. and S.T. are the inventors of patent applications for CD37CAR, submitted by Nagoya University, Nagoya, Japan.

REFERENCES

1. June, C.H., and Sadelain, M. (2018). Chimeric Antigen Receptor Therapy. N. Engl. J. Med. *379*, 64–73. https://doi.org/10.1056/NEJMra1706169.

2. Salter, A.I., Pont, M.J., and Riddell, S.R. (2018). Chimeric antigen receptor-modified T cells: CD19 and the road beyond. Blood *131*, 2621–2629. https://doi.org/10.1182/blood-2018-01-785840.

3. Davila, M.L., Riviere, I., Wang, X., Bartido, S., Park, J., Curran, K., Chung, S.S., Stefanski, J., Borquez-Ojeda, O., Olszewska, M., et al. (2014). Efficacy and toxicity management of 19-28z CAR T cell therapy in B cell acute lymphoblastic leukemia. Sci. Transl. Med. *6*, 224ra25. https://doi.org/10.1126/scitranslmed.3008226.

4. Maude, S.L., Frey, N., Shaw, P.A., Aplenc, R., Barrett, D.M., Bunin, N.J., Chew, A., Gonzalez, V.E., Zheng, Z., Lacey, S.F., et al. (2014). Chimeric antigen receptor T cells for sustained remissions in leukemia. N. Engl. J. Med. *371*, 1507–1517. https://doi.org/10.1056/NEJMoa1407222.

5. Lee, D.W., Kochenderfer, J.N., Stetler-Stevenson, M., Cui, Y.K., Delbrook, C., Feldman, S.A., Fry, T.J., Orentas, R., Sabatino, M., Shah, N.N., et al. (2015). T cells expressing CD19 chimeric antigen receptors for acute lymphoblastic leukaemia in children and young adults: a phase 1 dose-escalation trial. Lancet *385*, 517–528. https://doi.org/10.1016/S0140-6736(14)61403-3.

6. Abramson, J.S., Palomba, M.L., Gordon, L.I., Lunning, M.A., Wang, M., Arnason, J., Mehta, A., Purev, E., Maloney, D.G., Andreadis, C., et al. (2020). Lisocabtagene maraleucel for patients with relapsed or refractory large B-cell lymphomas (TRANSCEND NHL 001): a multicentre seamless design study. Lancet *396*, 839–852. https://doi.org/10.1016/S0140-6736(20)31366-0.

7. Porter, D.L., Hwang, W.T., Frey, N.V., Lacey, S.F., Shaw, P.A., Loren, A.W., Bagg, A., Marcucci, K.T., Shen, A., Gonzalez, V., et al. (2015). Chimeric antigen receptor T cells persist and induce sustained remissions in relapsed refractory chronic lymphocytic leukemia. Sci. Transl. Med. *7*, 303ra139. https://doi.org/10.1126/scitranslmed.aac5415.

8. Kochenderfer, J.N., Dudley, M.E., Kassim, S.H., Somerville, R.P.T., Carpenter, R.O., Stetler-Stevenson, M., Yang, J.C., Phan, G.Q., Hughes, M.S., Sherry, R.M., et al. (2015). Chemotherapy-refractory diffuse large B-cell lymphoma and indolent B-cell malignancies can be effectively treated with autologous T cells expressing an anti-CD19 chimeric antigen receptor. J. Clin. Oncol. *33*, 540–549. https://doi.org/10.1200/JCO.2014.56.2025.

9. Schuster, S.J., Svoboda, J., Chong, E.A., Nasta, S.D., Mato, A.R., Anak, Ö., Brogdon, J.L., Pruteanu-Malinici, I., Bhoj, V., Landsburg, D., et al. (2017). Chimeric Antigen Receptor T Cells in Refractory B-Cell Lymphomas. N. Engl. J. Med. *377*, 2545–2554. https://doi.org/10.1056/NEJMoa1708566.

10. Neelapu, S.S., Locke, F.L., Bartlett, N.L., Lekakis, L.J., Miklos, D.B., Jacobson, C.A., Braunschweig, I., Oluwole, O.O., Siddiqi, T., Lin, Y., et al. (2017). Axicabtagene Ciloleucel CAR T-Cell Therapy in Refractory Large B-Cell Lymphoma. N. Engl. J. Med. *377*, 2531–2544. https://doi.org/10.1056/NEJMoa1707447.

11. Turtle, C.J., Hay, K.A., Hanafi, L.A., Li, D., Cherian, S., Chen, X., Wood, B., Lozanski, A., Byrd, J.C., Heimfeld, S., et al. (2017). Durable Molecular Remissions in Chronic Lymphocytic Leukemia Treated With CD19-Specific Chimeric Antigen Receptor-Modified T Cells After Failure of Ibrutinib. J. Clin. Oncol. *35*, 3010–3020. https://doi.org/10.1200/JCO.2017.72.8519.

12. Rafiq, S., Hackett, C.S., and Brentjens, R.J. (2020). Engineering strategies to overcome the current roadblocks in CAR T cell therapy. Nat. Rev. Clin. Oncol. *17*, 147–167. https://doi.org/10.1038/s41571-019-0297-y.

13. Li, G., Boucher, J.C., Kotani, H., Park, K., Zhang, Y., Shrestha, B., Wang, X., Guan, L., Beatty, N., Abate-Daga, D., and Davila, M.L. (2018). 4-1BB enhancement of CAR T function requires NF-κB and TRAFs. JCI Insight *3*, e121322. https://doi.org/10.1172/jci.insight.121322.

14. Gaud, G., Lesourne, R., and Love, P.E. (2018). Regulatory mechanisms in T cell receptor signalling. Nat. Rev. Immunol. *18*, 485–497. https://doi.org/10.1038/s41577-018-0020-8.

15. Bishop, G.A., Warren, W.D., and Berton, M.T. (1995). Signaling via major histocompatibility complex class II molecules and antigen receptors enhances the B cell response to gp39/CD40 ligand. Eur. J. Immunol. *25*, 1230–1238. https://doi.org/10.1002/eji.1830250515.

16. Haxhinasto, S.A., Hostager, B.S., and Bishop, G.A. (2002). Cutting edge: molecular mechanisms of synergy between CD40 and the B cell antigen receptor: role for TNF receptor-associated factor 2 in receptor interaction. J. Immunol. *169*, 1145–1149.

17. Haxhinasto, S.A., and Bishop, G.A. (2004). Synergistic B cell activation by CD40 and the B cell antigen receptor: role of B lymphocyte antigen receptor-mediated kinase activation and tumor necrosis factor receptor-associated factor regulation. J. Biol. Chem. *279*, 2575–2582. https://doi.org/10.1074/jbc.M310628200.

18. Munroe, M.E., and Bishop, G.A. (2007). A costimulatory function for T cell CD40. J. Immunol. *178*, 671–682.

19. Sun, S.C. (2017). The non-canonical NF-κB pathway in immunity and inflammation. Nat. Rev. Immunol. *17*, 545–558. https://doi.org/10.1038/nri.2017.52.

20. Sun, S.C. (2011). Non-canonical NF-κB signaling pathway. Cell Res. *21*, 71–85. https://doi.org/10.1038/cr.2010.177.

21. Zhao, Z., Condomines, M., van der Stegen, S.J.C., Perna, F., Kloss, C.C., Gunset, G., Plotkin, J., and Sadelain, M. (2015). Structural Design of Engineered Costimulation Determines Tumor Rejection Kinetics and Persistence of CAR T Cells. Cancer Cell *28*, 415–428. https://doi.org/10.1016/j.ccell.2015.09.004.

22. Julamanee, J., Terakura, S., Umemura, K., Adachi, Y., Miyao, K., Okuno, S., Takagi, E., Sakai, T., Koyama, D., Goto, T., et al. (2021). Composite CD79A/CD40 co-stimulatory endodomain enhances CD19CAR-T cell proliferation and survival. Mol. Ther. *29*, 2677–2690. https://doi.org/10.1016/j.ymthe.2021.04.038.

23. Jutz, S., Leitner, J., Schmetterer, K., Doel-Perez, I., Majdic, O., Grabmeier-Pfistershammer, K., Paster, W., Huppa, J.B., and Steinberger, P. (2016). Assessment of costimulation and coinhibition in a triple parameter T cell reporter line: Simultaneous measurement of NF-κB, NFAT and AP-1. J. Immunol. Methods *430*, 10–20. https://doi.org/10.1016/j.jim.2016.01.007.

24. Rydzek, J., Nerreter, T., Peng, H., Jutz, S., Leitner, J., Steinberger, P., Einsele, H., Rader, C., and Hudecek, M. (2019). Chimeric Antigen Receptor Library Screening Using a Novel NF-κB/NFAT Reporter Cell Platform. Mol. Ther. *27*, 287–299. https://doi.org/10.1016/j.ymthe.2018.11.015.

25. Larson, R.C., and Maus, M.V. (2021). Recent advances and discoveries in the mechanisms and functions of CAR T cells. Nat. Rev. Cancer *21*, 145–161. https://doi.org/10.1038/s41568-020-00323-z.

26. Hayden, M.S., and Ghosh, S. (2008). Shared principles in NF-kappaB signaling. Cell *132*, 344–362. https://doi.org/10.1016/j.cell.2008.01.020.

27. Philipson, B.I., O'Connor, R.S., May, M.J., June, C.H., Albelda, S.M., and Milone, M.C. (2020). 4-1BB costimulation promotes CAR T cell survival through noncanonical NF-κB signaling. Sci. Signal. *13*, eaay8248. https://doi.org/10.1126/scisignal.aay8248.

28. Macián, F., García-Cózar, F., Im, S.H., Horton, H.F., Byrne, M.C., and Rao, A. (2002). Transcriptional mechanisms underlying lymphocyte tolerance. Cell *109*, 719–731. https://doi.org/10.1016/s0092-8674(02)00767-5.

29. Wherry, E.J., Ha, S.J., Kaech, S.M., Haining, W.N., Sarkar, S., Kalia, V., Subramaniam, S., Blattman, J.N., Barber, D.L., and Ahmed, R. (2007). Molecular signature of CD8+ T cell exhaustion during chronic viral infection. Immunity *27*, 670–684. https://doi.org/10.1016/j.immuni.2007.09.006.

30. Martinez, G.J., Pereira, R.M., Äijö, T., Kim, E.Y., Marangoni, F., Pipkin, M.E., Togher, S., Heissmeyer, V., Zhang, Y.C., Crotty, S., et al. (2015). The transcription factor NFAT promotes exhaustion of activated CD8⁺ T cells. Immunity *42*, 265–278. https://doi.org/10.1016/j.immuni.2015.01.006.

31. Huang, W., Lin, W., Chen, B., Zhang, J., Gao, P., Fan, Y., Lin, Y., and Wei, P. (2023). NFAT and NF-κB dynamically co-regulate TCR and CAR signaling responses in human T cells. Cell Rep. *42*, 112663. https://doi.org/10.1016/j.celrep.2023.112663.

32. Caballero, A.C., Escribà-Garcia, L., Alvarez-Fernández, C., and Briones, J. (2022). CAR T-Cell Therapy Predictive Response Markers in Diffuse Large B-Cell Lymphoma and Therapeutic Options After CART19 Failure. Front. Immunol. *13*, 904497. https://doi.org/10.3389/fimmu.2022.904497.

33. Levin-Piaeda, O., Levin, N., Pozner, S., Danieli, A., Weinstein-Marom, H., and Gross, G. (2021). The Intracellular Domain of CD40 is a Potent Costimulatory Element in Chimeric Antigen Receptors. J. Immunother. *44*, 209–213. https://doi.org/10.1097/CJI.0000000000000373.

34. Escobar, G., Mangani, D., and Anderson, A.C. (2020). T cell factor 1: A master regulator of the T cell response in disease. Sci. Immunol. *5*, eabb9726. https://doi.org/10.1126/sciimmunol.abb9726.

35. He, R., Hou, S., Liu, C., Zhang, A., Bai, Q., Han, M., Yang, Y., Wei, G., Shen, T., Yang, X., et al. (2016). Follicular CXCR5- expressing CD8(+) T cells curtail chronic viral infection. Nature *537*, 412–428. https://doi.org/10.1038/nature19317.

36. Leong, Y.A., Chen, Y., Ong, H.S., Wu, D., Man, K., Deleage, C., Minnich, M., Meckiff, B.J., Wei, Y., Hou, Z., et al. (2016). CXCR5(+) follicular cytotoxic T cells control viral infection in B cell follicles. Nat. Immunol. *17*, 1187–1196. https://doi.org/10.1038/ni.3543.

37. Zou, Y., Liu, B., Li, L., Yin, Q., Tang, J., Jing, Z., Huang, X., Zhu, X., and Chi, T. (2022). IKZF3 deficiency potentiates chimeric antigen receptor T cells targeting solid tumors. Cancer Lett. *524*, 121–130. https://doi.org/10.1016/j.canlet.2021.10.016.

38. Zhang, X., Zhang, C., Qiao, M., Cheng, C., Tang, N., Lu, S., Sun, W., Xu, B., Cao, Y., Wei, X., et al. (2022). Depletion of BATF in CAR-T cells enhances antitumor activity by inducing resistance against exhaustion and formation of central memory cells. Cancer Cell *40*, 1407–1422.e7. https://doi.org/10.1016/j.ccell.2022.09.013.

39. Almeida, L., Lochner, M., Berod, L., and Sparwasser, T. (2016). Metabolic pathways in T cell activation and lineage differentiation. Semin. Immunol. *28*, 514–524. https://doi.org/10.1016/j.smim.2016.10.009.

40. Kawalekar, O.U., O' Connor, R.S., Fraietta, J.A., Guo, L., McGettigan, S.E., Posey, A.D., Patel, P.R., Guedan, S., Scholler, J., Keith, B., et al. (2016). Distinct Signaling of Coreceptors Regulates Specific Metabolism Pathways and Impacts Memory Development in CAR T Cells. Immunity *44*, 712. https://doi.org/10.1016/j.immuni.2016.02.023.

41. van der Stegen, S.J.C., Hamieh, M., and Sadelain, M. (2015). The pharmacology of second-generation chimeric antigen receptors. Nat. Rev. Drug Discov. *14*, 499–509. https://doi.org/10.1038/nrd4597.

42. Alaggio, R., Amador, C., Anagnostopoulos, I., Attygalle, A.D., Araujo, I.B.d.O., Berti, E., Bhagat, G., Borges, A.M., Boyer, D., Calaminici, M., et al. (2022). The 5th edition of the World Health Organization Classification of Haematolymphoid Tumours: Lymphoid Neoplasms. Leukemia *36*, 1720–1748. https://doi.org/10.1038/s41375-022-01620-2.

43. Okuno, S., Adachi, Y., Terakura, S., Julamanee, J., Sakai, T., Umemura, K., Miyao, K., Goto, T., Murase, A., Shimada, K., et al. (2021). Spacer Length Modification Facilitates Discrimination between Normal and Neoplastic Cells and Provides Clinically Relevant CD37 CAR-T Cells. J. Immunol. *206*, 2862–2874. https://doi.org/10.4049/jimmunol.2000768.

44. Guedan, S., Posey, A.D., Shaw, C., Wing, A., Da, T., Patel, P.R., McGettigan, S.E., Casado-Medrano, V., Kawalekar, O.U., Uribe-Herranz, M., et al. (2018). Enhancing CAR T cell persistence through ICOS and 4-1BB costimulation. JCI Insight *3*, e96976. https://doi.org/10.1172/jci.insight.96976.

45. Si, W., Fan, Y.Y., Qiu, S.Z., Li, X., Wu, E.Y., Ju, J.Q., Huang, W., Wang, H.P., and Wei, P. (2023). Design of diversified chimeric antigen receptors through rational module recombination. iScience *26*, 106529. https://doi.org/10.1016/j.isci.2023.106529.

46. Terakura, S., Yamamoto, T.N., Gardner, R.A., Turtle, C.J., Jensen, M.C., and Riddell, S.R. (2012). Generation of CD19-chimeric antigen receptor modified CD8+ T cells derived from virus-specific central memory T cells. Blood *119*, 72–82. https://doi.org/10.1182/blood-2011-07-366419.

47. Kowolik, C.M., Topp, M.S., Gonzalez, S., Pfeiffer, T., Olivares, S., Gonzalez, N., Smith, D.D., Forman, S.J., Jensen, M.C., and Cooper, L.J.N. (2006). CD28 costimulation provided through a CD19-specific chimeric antigen receptor enhances in vivo persistence and antitumor efficacy of adoptively transferred T cells. Cancer Res. *66*, 10995–11004. https://doi.org/10.1158/0008-5472.CAN-06-0160.

48. Wang, X., Chang, W.C., Wong, C.W., Colcher, D., Sherman, M., Ostberg, J.R., Forman, S.J., Riddell, S.R., and Jensen, M.C. (2011). A transgene-encoded cell surface polypeptide for selection, in vivo tracking, and ablation of engineered cells. Blood *118*, 1255–1263. https://doi.org/10.1182/blood-2011-02-337360.

49. Watanabe, K., Terakura, S., Martens, A.C., van Meerten, T., Uchiyama, S., Imai, M., Sakemura, R., Goto, T., Hanajiri, R., Imahashi, N., et al. (2015). Target antigen density governs the efficacy of anti-CD20-CD28-CD3 ζ chimeric antigen receptor-modified effector CD8+ T cells. J. Immunol. *194*, 911–920. https://doi.org/10.4049/jimmunol.1402346.

50. Khopanlert, W., Jangphattananont, N., Maneechai, K., Ung, S., Viboonjuntra, P., Terakura, S., and Julamanee, J. (2022). The novel dual T/B-cell signaling molecule confers the greater tumoricidal activity and T-cell persistence of CD19 chimeric antigen receptor T-cell. Hemasphere *6*, 1432.

51. Khopanlert, W., Choochuen, P., Jangphattananont, N., Maneechai, K., Ung, S., Sangkhathat, S., Viboonjuntra, P., Terakura, S., and Julamanee, J. (2022). Co-Stimulation of CD28/CD40 Signaling Molecule Potentiates CD19CAR-T Cell Functions and Stemness. Blood *140*, 7364–7365. https://doi.org/10.1182/blood-2022-156967.